Lin et al., http://www.jcb.org/cgi/content/full/jcb.201209098/DC1

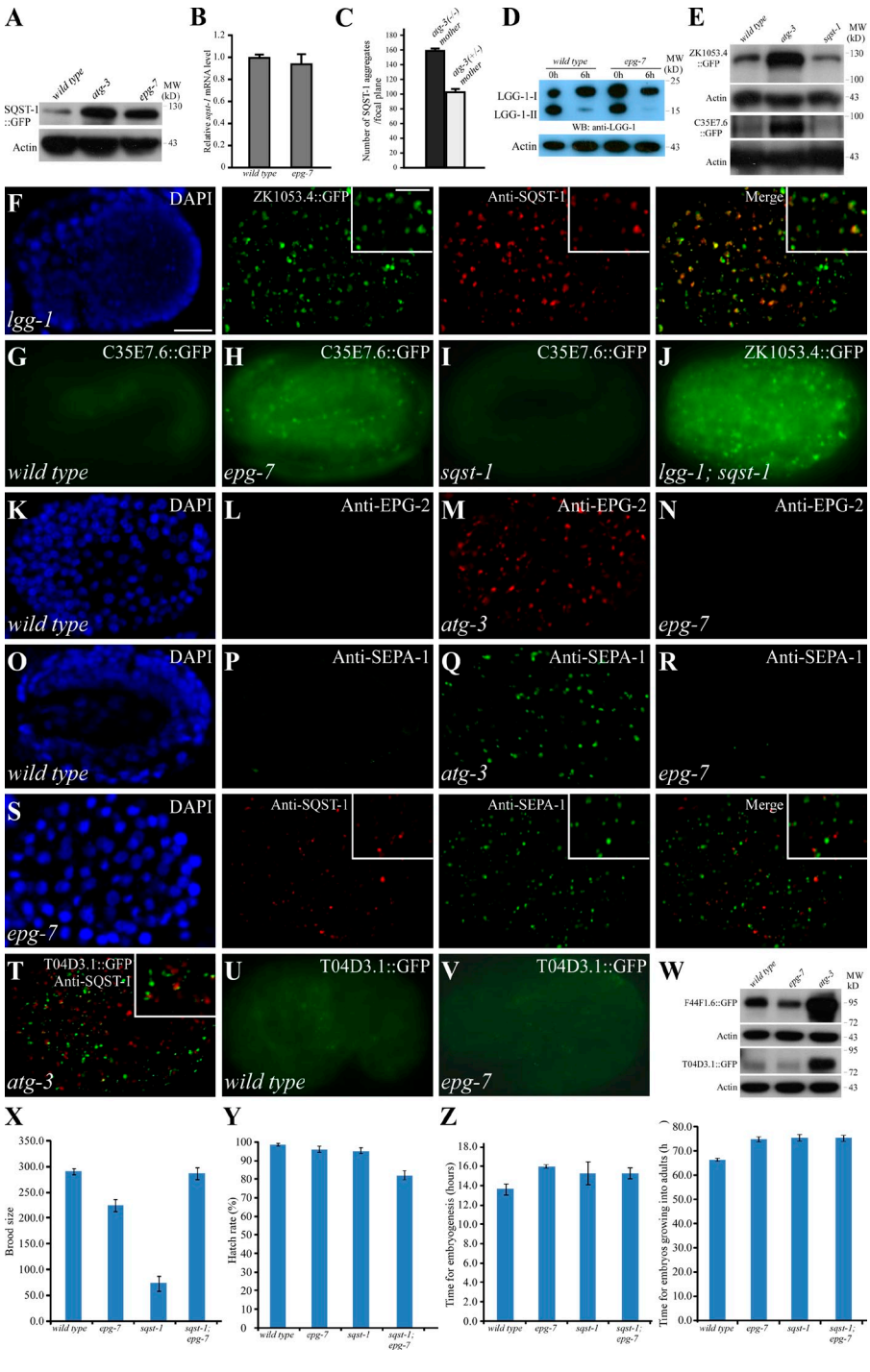

Figure S1. **Loss of *epg-7* function causes defective degradation of SQST-1–containing aggregates.** (A) Levels of SQST-1::GFP are dramatically elevated in *atg-3* and *epg-7* mutants compared with wild-type embryos in an immunoblotting assay. (B) The *sqst-1* mRNA level remains unchanged in wild-type and *epg-7* mutant embryos. Real-time PCR was performed to determine the mRNA level. Actin was used as an internal control. (C) Average number of SQST-1 aggregates per focal plane in *atg-3* mutant embryos derived from heterozygous (*atg-3*$^{+/-}$) or homozygous (*atg-3*$^{-/-}$) mother at the ∼100-cell stage. Autophagy mutants show a maternal effect on degradation of oocyte-derived P granules (Zhang et al., 2009). Thus, early stage embryos may contain a high level of autophagy activity contributed by the oocyte. (D) Levels of LGG-1 in embryos derived from newly bleached hermaphrodites (early stage embryos) or in embryos 6 h after bleach (late stage embryos). (E) Compared with wild-type embryos, levels of ZK1053.4::GFP and C35E7.6::GFP are dramatically elevated in *atg-3* mutants, but remain unchanged in *sqst-1* mutants in an immunoblotting assay. (F) In *lgg-1* mutants, ZK1053.4::GFP forms many aggregates that colocalize with SQST-1. Insets show a magnified view. (G) In a wild-type embryo, C35E7.6::GFP is weakly expressed and diffusely localized in the cytoplasm. (H) C35E7.6::GFP accumulates into a large number of aggregates in *epg-7* mutant embryos. (I) Loss of function of *sqst-1* has no effect on the expression of C35E7.6::GFP. (J) Loss of *sqst-1* has no effect on the formation of ZK1053.4::GFP aggregates in *lgg-1* mutants. (K and L) In a wild-type embryo, EPG-2 aggregates are absent at the comma stage. (K) DAPI image of the embryo shown in L. (M) EPG-2 accumulates into a large number of aggregates in an *atg-3* mutant embryo at the comma stage. (N) No accumulation of EPG-2 aggregates in an *epg-7* comma stage embryo. (O and P) SEPA-1 aggregates are absent in wild-type embryos at the fourfold stage. (O) DAPI image of the embryo shown in P. (Q) SEPA-1 accumulates into a large number of aggregates in an *atg-3* mutant embryo at the fourfold stage. (R) No SEPA-1 aggregates are formed in an *epg-7* mutant embryo at the fourfold stage. (S) SQST-1 aggregates are separable from SEPA-1 aggregates in *epg-7* mutant embryos. (T) T04D3.1 aggregates are separable from SQST-1 aggregates in *atg-3* mutants. (U and V) T04D3.1::GFP is expressed at the same level in wild-type embryos (U) and *epg-7* mutant embryos (V). (W) Compared with wild-type embryos, levels of F44F1.6 and T04D3.1 are dramatically elevated in *atg-3* mutants, but remain unchanged in *epg-7* mutants in an immunoblotting assay. (X) Brood size (number of embryos produced by one hermaphrodite) in wild-type, *epg-7*, *sqst-1*, and *sqst-1;epg-7* animals. (P value: wild type vs. *epg-7* = 0.02; *epg-7* vs. *sqst-1;epg-7* = 0.04; wild type vs. *sqst-1;epg-7* = 0.38). (Y) L1 hatch rate (percentage of embryos developing into larvae) in wild-type, *epg-7*, *sqst-1*, and *sqst-1;epg-7* animals. (P value: wild type vs. *epg-7* = 0.06; wild type vs. *sqst-1* = 0.01; *epg-7* vs. *sqst-1;epg-7* = 0.007; wild type vs. *sqst-1;epg-7* = 0.007). (Z) Time (hours) for embryos developing into L1 larvae or growing into young adults in wild-type, *epg-7*, *sqst-1*, and *sqst-1;epg-7* animals (for developing into larvae, P value: wild type vs. *epg-7* = 0.01; wild type vs. *sqst-1* = 0.20; *epg-7* vs. *sqst-1;epg-7* = 0.18; for growing into adults, P value: wild type vs. *epg-7* = 0.01; wild type vs. *sqst-1* = 0.004; *epg-7* vs. *sqst-1;epg-7* = 0.42). Bars: (F–V) 10 µm; (insets in F, S, and T) 5 µm. *C. elegans* embryos remain the same size during embryogenesis and loss of autophagy activity has no effect on the embryo size. Thus, bars for embryos are only shown once in each figure.

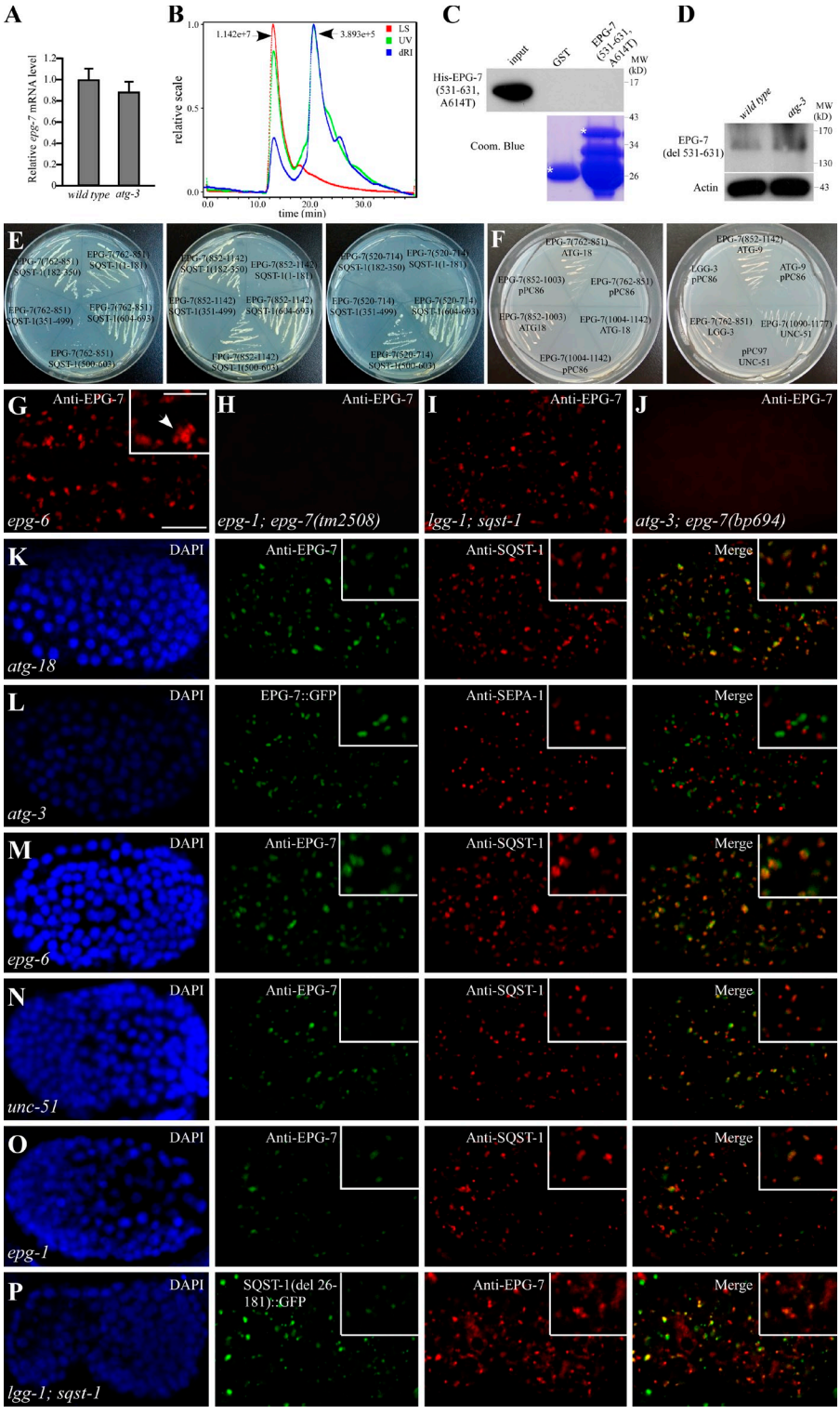

Figure S2. **EPG-7 is degraded by autophagy and colocalizes with SQST-1 aggregates in autophagy mutants.** (A) Levels of *epg-7* mRNA are the same as wild type in *atg-3* mutants. (B) The size-exclusion chromatography and static light scattering assay indicates that EPG-7(520–714) forms oligomers. The x axis represents the elution time. The parameters monitored by LS (light scattering) and RI (refractive index) detectors are plotted as curves. The molecular weight corresponding to the peaks was calculated according to LS and RI measurements. Peak 1: 1.142e+7. Peak 2: 3.893e+5. LS, laser-light scattering; UV, ultraviolet light; dRI, differential refractive index. (C) Mutant EPG-7 proteins containing the *bp694* A614T mutation fail to self-interact. (D) Levels of EPG-7(del 531–631)::GFP remained unchanged in *atg-3* mutants. (E) Yeast two-hybrid assays to delineate the region in EPG-7 that contains SQST-1 binding activity. cDNAs encoding fragments of EPG-7 and SQST-1 were cloned into pPC97 and pPC86, respectively. (F) Yeast two-hybrid assays to delineate the region in EPG-7 that interacts with ATG proteins. cDNAs encoding fragments of EPG-7 were cloned into pPC97 and pPC86. cDNAs encoding LGG-3 and ATG-9 were cloned into pPC97. cDNAs encoding ATG-18 and UNC-51 were cloned into pPC86. (G) EPG-7 forms numerous aggregates in *epg-6* mutant embryos. EPG-7 aggregates are enlarged and form clusters (arrow) in *epg-6* mutants. Insets show a magnified view. (H) EPG-7 aggregates are absent in *epg-1;epg-7(tm2508)* mutants, confirming the specificity of the anti–EPG-7 antibody. (I) EPG-7 forms aggregates in *lgg-1;sqst-1* mutant embryos. (J) No EPG-7 aggregates are detected in *atg-3;epg-7(bp694)* mutant embryos. (K) EPG-7 forms a large number of aggregates that colocalize with SQST-1 aggregates in *atg-18* mutants. (L) EPG-7::GFP aggregates are separable from SEPA-1 aggregates in *atg-3* mutants. (M) EPG-7 and SQST-1 aggregates are enlarged and colocalized in *epg-6* mutants. (N and O) EPG-7 aggregates partially colocalize with SQST-1 aggregates in *unc-51* (N) and *epg-1* (O) mutants. Some EPG-7 aggregates are closely associated with, but do not overlap, the SQST-1 aggregates. Embryos at the ∼200-cell stage are shown in K–O. (P) SQST-1(del 26–181)::GFP aggregates colocalize with EPG-7 aggregates in *lgg-1;sqst-1* mutant embryos. Bars: (G–P) 10 µm; (insets in G–P) 5 µm.

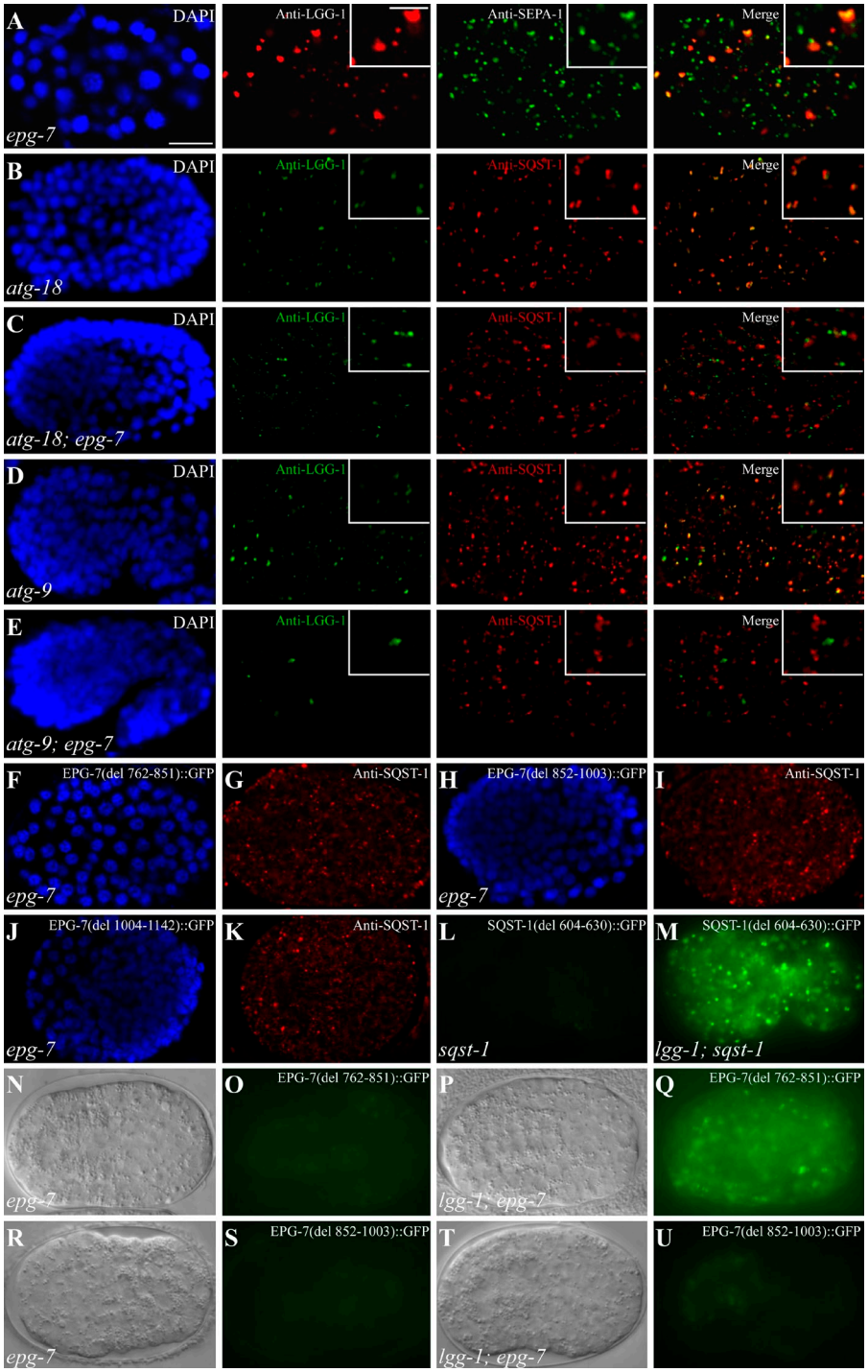

Figure S3. **Localization of SQST-1 aggregates and LGG-1 puncta in various autophagy mutants.** (A) SEPA-1 aggregates partially colocalize with the LGG-1 puncta in *epg-7* early stage mutant embryos. Insets show a magnified view. (B) In *atg-18* mutants, LGG-1 forms small punctate structures. LGG-1 puncta co-localize with SQST-1 aggregates at the ~200-cell stage onwards. (C) SQST-1 aggregates are separable from LGG-1 puncta in *atg-18;epg-7* mutants at the ~200-cell stage. (D) SQST-1 largely colocalizes with LGG-1 puncta in *atg-9* mutant embryos at the comma stage. (E) Loss of function of *epg-7* disrupts the colocalization of SQST-1 aggregates with LGG-1 puncta in *atg-9* mutants at the comma stage. Each DAPI image is of the embryo in the same row. (F–K) SQST-1 aggregates accumulate in *epg-7* mutants carrying an *epg-7(del 762–851)::gfp*, *epg-7(del 852–1003)::gfp*, or *epg-7(del 1004–1142)::gfp* transgene, in which ATG-binding motifs are deleted. (F, H, and J) DAPI images of the embryos shown in G, I, and K, respectively. (L and M) SQST-1(del 604–630)::GFP is weakly expressed and diffusely localized in the cytoplasm in *sqst-1(ok2892)* mutants (L). Loss of function of *lgg-1* dramatically elevates the expression level of SQST-1(del 604–630)::GFP, which forms a large number of aggregates (M). (N and O) EPG-7(del 762–851)::GFP is weakly expressed and diffusely localized in the cytoplasm in *epg-7* mutants. (P and Q) The expression level of EPG-7(del 762–851)::GFP is dramatically elevated and forms a large number of aggregates in *lgg-1* mutants. (R–U) EPG-7(del 852–1003)::GFP is weakly expressed and diffusely localized in the cytoplasm (R and S) and its expression level is not affected by loss of *lgg-1* activity (T and U). (N, P, R, and T) DIC images of the embryos shown in O, Q, S, and U, respectively. Bars: (A–U) 10 µm; (insets in A–E) 5 µm.

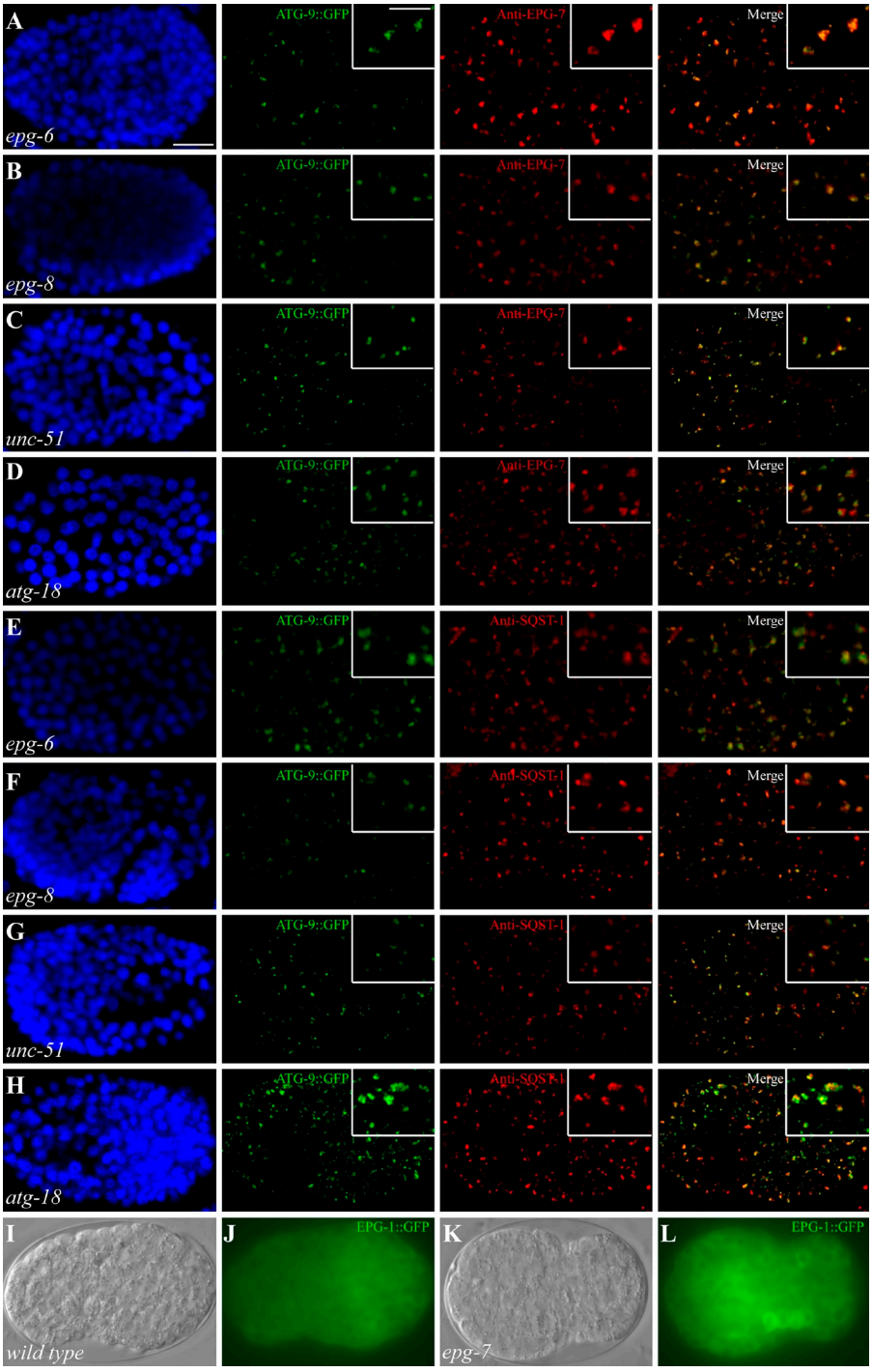

Figure S4. **Relationship of ATG-9::GFP with EPG-7 aggregates and SQST-1 aggregates in various autophagy mutants.** (A–D) Separate images for Fig. 6, Q–T. Insets show a magnified view. (E–H) Separate images for Fig. 6, U–X. Each DAPI image is of the embryo in the same row. (I and J) EPG-1::GFP is diffusely localized in the cytoplasm in a wild-type embryo. (K and L) Loss of function of *epg-7* does not evidently affect the pattern of EPG-1::GFP. (I and K) DIC images of the embryos shown in J and L, respectively. Bars: (A–L) 10 µm; (insets in A–H) 5 µm.

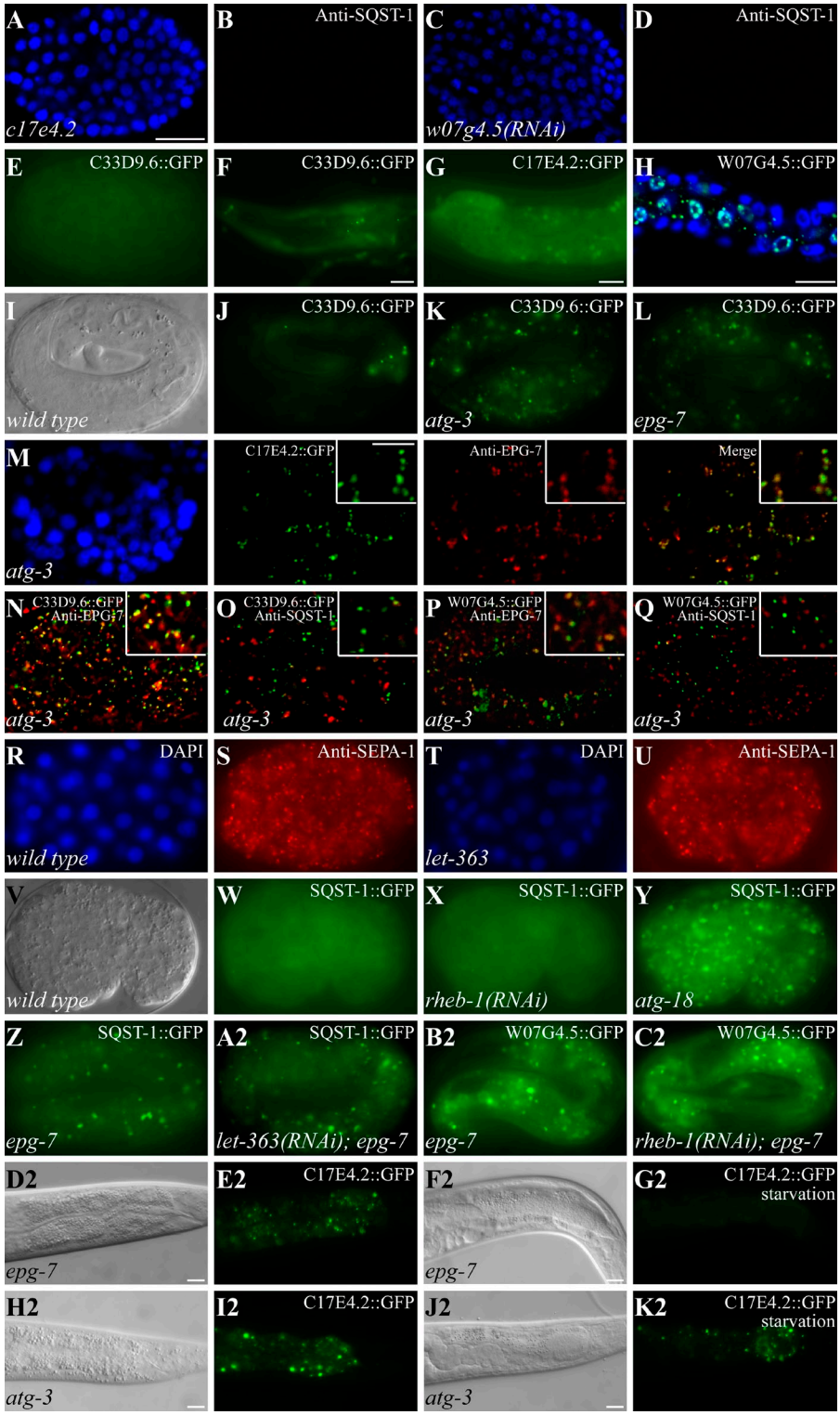

Figure S5. **EPG-7 mediates autophagic degradation of several other types of protein aggregates and is dispensable for starvation-induced autophagic degradation of substrate proteins.** (A–D) Loss of function of *c17e4.2* (A and B) or *w07g4.5* (C and D) does not cause a defect in degradation of SQST-1. No SQST-1 aggregates are detected in any stages of embryos. (A and C) DAPI images of the embryos shown in B and D, respectively. (E) C33D9.6::GFP is weakly expressed and diffusely localized in the cytoplasm of early stage embryos. (F) At larval stages, C33D9.6::GFP is largely diffusely localized apart from a few aggregates in hypodermal cells. (G) At the post-embryonic stage, C17E4.2::GFP is localized in the intestine and forms a few aggregates. (H) At larval stages, W07G4.5::GFP forms aggregates that are localized in the cytoplasm and also in the nuclei (blue) in intestinal cells. (I and J) In wild-type embryos, C33D9.6::GFP is weakly expressed and diffusely localized in the cytoplasm apart from a few punctate structures. (I) DIC image of the embryo shown in J. (K and L) C33D9.6::GFP is present at dramatically increased levels and forms a large number of aggregates in *atg-3* (K) and *epg-7* (L) mutant embryos. (M) Separate images for Fig. 7 J. C17E4.2::GFP aggregates colocalize with EPG-7 aggregates in *atg-3* mutants. Insets show a magnified view. (N and O) C33D9.6::GFP punctate structures overlap with EPG-7 aggregates (N) but are separable from SQST-1 aggregates (O) in *atg-3* mutants. (P and Q) In *atg-3* mutants, W07G4.5 punctate structures are largely colocalize with EPG-7 aggregates (P) but separable from SQST-1 aggregates (Q). (R and S) In wild-type embryos, a large number of SEPA-1 aggregates are present at the ~100-cell stage. (R) DAPI image of the embryo shown in S. (T and U) A large number of SEPA-1 aggregates accumulate in *let-363* mutant embryos, derived from *let-363(ok3018) I/hT2[bli-4(e937) let-?(q782) qIs48](I;III)*. (T) DAPI image of the embryo shown in U. (V–X) SQST-1 is weakly expressed in wild-type embryos (V and W) and its expression level remains unchanged in *rheb-1(RNAi)* embryos (X). (Y) SQST-1 accumulates into a large number of aggregates in *atg-18* mutant embryos. (Z) SQST-1 forms aggregates in *epg-7* mutant embryos. (A2) Expression of SQST-1 in *epg-7* mutant embryos is not affected by inactivation of *let-363*. (B2 and C2) W07G4.5::GFP forms a large number of aggregates in *epg-7* mutant embryos. Simultaneously depleting *rheb-1* activity has no effect on the expression of aggregates. (D2–G2) C17E4.2::GFP accumulates into many aggregates in the intestine in *epg-7* mutants (D2 and E2), which disappear after starvation treatment (F2 and G2). (H2–K2) C17E4.2::GFP aggregates in the intestine in *atg-3* mutant larvae are not affected after starvation treatment. (D2, F2, H2, and J2) DIC images of the embryos shown in E2, G2, I2, and K2, respectively. Bars: (A–E and I–C2) 10 µm; (insets in M–Q) 5 µm; (F–H) 10 µm; (D2–K2) 10 µm.

Table S1. **Autophagy genes in yeast, *C. elegans*, and mammals**

Yeast *ATG* gene	*C. elegans ATG* homologue	Mammalian *ATG* homologue
atg1	*unc-51*	*ULK1*
atg13	*epg-1*	*ATG13*
atg17	–	*FIP200*
–	*epg-9*	*ATG101*
vps34	*vps-34*	*VPS34*
atg6	*bec-1*	*BECLIN1*
atg14	*epg-8*	*ATG14L*
atg4	*atg-4.1, atg-4.2*	*ATG4A, ATG4B, ATG4C, ATG4D*
atg3	*atg-3*	*ATG3*
atg7	*atg-7*	*ATG7*
atg8	*lgg-1/lgg-2*	*LC3, GATE16, GABARAP*
atg5	*atg-5*	*ATG5*
atg10	*atg-10*	*ATG10*
atg12	*lgg-3*	*ATG12*
atg16	*atg-16.1, atg-16.2*	*ATG16L*
atg18	*atg-18, epg-6*	*WIPI1-4*
atg2	*atg-2*	*ATG2A, ATG2B*
atg9	*atg-9*	*ATG9*
–	*epg-3*	*VMP1*
–	*epg-4*	*EI24*
–	*epg-5*	*mEPG5*
–	*epg-2*	–
–	*epg-7*	–

Reference

Zhang, Y.X., L.B. Yan, Z. Zhou, P.G. Yang, E. Tian, K. Zhang, Y. Zhao, Z.P. Li, B. Song, J.H. Han, et al. 2009. SEPA-1 mediates the specific recognition and degradation of P granule components by autophagy in *C. elegans. Cell*. 136:308–321. http://dx.doi.org/10.1016/j.cell.2008.12.022